# Gravitational Waves from Relativistic Neutron-Star Mergers with Microphysical Equations of State

R. Oechslin and H.-T. Janka

*Max-Planck-Institut für Astrophysik, Karl-Schwarzschild-Strasse 1, D-85741 Garching, Germany*
(Received 9 February 2007; published 19 September 2007)

The gravitational wave (GW) emission from a set of relativistic neutron-star (NS) merger simulations is analyzed and characteristic signal features are identified. The distinct peak in the GW energy spectrum that is associated with the formation of a hypermassive merger remnant has a frequency that depends strongly on the properties of the nuclear equation of state (EOS) and on the total mass of the binary system, whereas the mass ratio and the NS spins have a weak influence. If the total mass can be determined from the inspiral chirp signal, the peak frequency of the post-merger signal is a sensitive indicator of the EOS.

Among the strongest known sources of gravitational wave (GW) emission are the merging events of double neutron-star (DNS) binaries. Recent population synthesis studies (e.g., [1]) and the discovery of the DNS J0737-3039 [2] suggest a possible detection rate of GW radiation from DNS mergers of one in $\sim 30$ y for Laser Interferometer Gravitational Wave Observatory (LIGO I) and one every two days for advanced LIGO. To detect such GW signals and to filter them out of the detector output, theoretical waveform templates are needed. While the inspiral phase prior to the actual merger can be described very accurately within the post-Newtonian (PN) framework (e.g., [3]), hydrodynamical simulations are needed to model the dynamical merging phase. In addition, different aspects of physics enter the problem at this stage. Besides general relativity (GR), nuclear and particle physics play a role in the description of the hot and dense NS fluid via an equation of state (EOS) and in the treatment of energy losses (e.g., by neutrinos) after the merging. The GW signal of the late inspiral and merging phases is therefore expected to contain information not only on the binary parameters such as masses and spins but also on the nuclear EOS.

Efforts to investigate NS mergers have concentrated either on the relativistic aspects while simplifying the microphysics (e.g., [4] and references therein), or have employed a microphysical EOS together with an approximative neutrino treatment while describing gravity in a Newtonian framework (e.g., [5,6]). The conformal flatness approach, a middle ground between PN and full GR, combined with a nuclear physics-based nonzero-temperature ($T \neq 0$) EOS has recently been chosen by Oechslin *et al.* [7].

The generic GW signal from a NS merger can be split into a chirplike part emitted by the inspiraling binary, the burst amplitude from the final plunge when the two stars collide (when time is set to $t = 0$ in Fig. 1), and a quasi-periodic post-merger signal caused either by the rotation and internal oscillation of a newly formed, nonaxisymmetric hypermassive NS (HMNS) as merger remnant or by the quasinormal ringing of a newly born black hole (BH) in case of a prompt gravitational collapse of the remnant after the final plunge. A first maximum of the compactness of the relic HMNS is associated with a minimum of the amplitude $h = (|h_+|^2 + |h_\times|^2)^{1/2}$ at about 0.5 ms after the merging, followed by the onset of the characteristically different, quasiperiodic post-merger emission. For some of our computed models, the quantity $h$ is plotted in Fig. 1. It contains the combined information from both polarizations $h_+$ and $h_\times$ of the wave amplitude and therefore represents the envelope of the high-frequency wave pattern. Its post-merger modulation is caused by the oscillation of the nonaxisymmetric remnant. Since the pre- and post-merger signals are emitted in different frequency bands, they can be clearly identified in the corresponding luminosity spec-
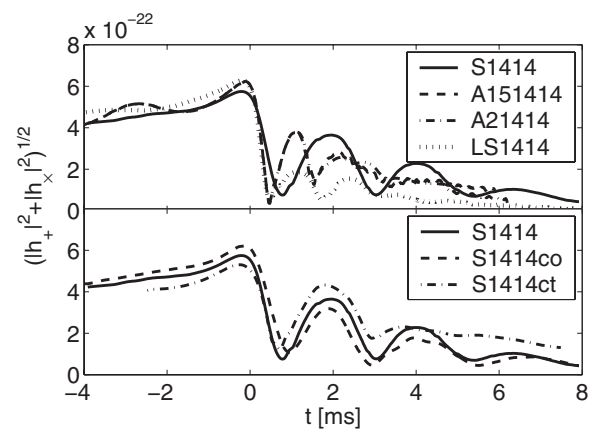


FIG. 1. The GW amplitude $h$ for different EOSs and spins as radiated perpendicularly to the orbital plane of the merging binary and measurable at a distance of 20 Mpc. The minimum at about 0.5 ms is considered to mark the onset of the quasiperiodic wave train caused by oscillations of the rapidly spinning, nonaxisymmetric merger remnant.

trum. The inspiral signal leads to a broadband contribution below ∼1 kHz and depends mainly on the NS masses and their spins, while an EOS dependence is only present in the very last stage before merging [8]. On the other hand, the post-merger signal is dominated by a quasiperiodic wave pattern with a frequency of about 2–4 kHz or about 6–7 kHz, depending on whether a HMNS forms or a prompt collapse to a BH happens [9]. The associated peak in the luminosity spectrum can become very pronounced in cases where the remnant keeps radiating GWs for several tens of ms as suggested by recent merger simulations [4,7]. The bare presence of a contribution in the frequency range of about 2–4 kHz indicates the formation of a HMNS and a nuclear EOS that is sufficiently stiff to prevent prompt BH formation.

In the present Letter, we concentrate on the HMNS formation case and assess the question, to which extent the nuclear EOS and the binary parameters can be constrained when such a post-merger peak is detected. Based on a set of simulated binary merger models [7], we identify characteristic features of the simulated GW signals and link them to the merger properties. The simulations were carried out with our relativistic smoothed particle hydrodynamics (SPH) code [10,11], which solves the relativistic hydrodynamics equations together with the Einstein field equation in the conformally flat approximation (CFC; [12,13]). The simulations were started from a stable equilibrium configuration slightly outside the innermost stable circular orbit and the corresponding initial data were generated by relaxing the fluid to a velocity field that includes the orbital motion and the proper spins of the NSs. Two $T \neq 0$ EOSs, the Shen-EOS [14] and the Lattimer-Swesty-EOS [15], an ideal-gas EOS with parameters chosen to mimic the Shen-EOS, and the APR-EOS [16] were used. The APR-EOS was extended by an ideal-gas-like thermal pressure contribution that is proportional to the internal energy increase due to shock heating and viscous heating [4]. The size of this contribution is determined by an adiabatic index $\Gamma_{th}$ for which we chose two different values ($\Gamma_{th} = 1.5, 2$) in order to investigate its influence on the merger outcome. Finally we calculated two models with the Shen-EOS, restricting the latter to $T = 0$ in order to investigate the influence of temperature-dependent pressure terms (see [7]).

The Shen-EOS is relatively stiff and for NSs with typical masses around $1.4M_\odot$ leads to radii as big as $R_{NS} \gtrsim 14$ km. Its maximum mass of nonrotating NSs is $\sim 2.25M_\odot$. In contrast, the LS-EOS is much softer and yields a radius near 12 km for a $1.4M_\odot$ NS. The APR-EOS is still softer below and around nuclear density, but becomes very stiff at higher densities ($\gtrsim 3 \times 10^{14}$ g cm$^{-3}$). Therefore, it makes NSs even more compact ($R_{NS} \sim 11$ km), although it allows for a rather large maximum NS mass of $\sim 2.2M_\odot$ compared to about $1.8M_\odot$ for the LS-EOS (see Fig. 2 in [7]). Besides the EOS, we have also varied the NS masses, the mass ratio, and the NS spins in our calculated set of models (see Table I).

TABLE I. Characteristic quantities of our computed models. Models with names starting with $S$ use the $T \neq 0$ Shen-EOS, $C$ models the restriction of this EOS to $T = 0$, the LS model uses the LS-EOS, the $P$ model the ideal-gas EOS, and the A15 and A2 models the APR-EOS extended by ideal gases with different values of $\Gamma_{th}$. All models were computed with irrotating initial conditions except the last four cases where the ending "co" ("ct") of the model names indicates initially corotating (counterrotating) spin states of the NSs (for the spin frequencies, see [7]). $M_1$ and $M_2$ are the individual gravitational masses in isolation, and $q = M_1/M_2$ is the mass ratio. $f_{max}$, $f_{peak}$, $\Delta E_{in}$, and $\Delta E_{pm}$ are defined in the text. SNR means the estimated signal-to-noise ratios in advanced LIGO (left) and DUAL (right) for the GW emission after merging and a source distance of 20 Mpc.

| Model | $M_1$ $M_\odot$ | $M_2$ $M_\odot$ | $q$ | $f_{peak}$ kHz | $f_{max}$ kHz | $\Delta E_{in}$ $10^{-3}M_\odot$ | $\Delta E_{pm}$ | SNR | |
|---|---|---|---|---|---|---|---|---|---|
| S1414 | 1.4 | 1.4 | 1.0 | 2.24 | 1.31 | 6.2 | 5.3 | 2.7 | 3.2 |
| S135145 | 1.35 | 1.45 | 0.93 | 2.27 | 1.35 | 6.2 | 6.4 | 2.8 | 3.3 |
| S1315 | 1.3 | 1.5 | 0.87 | 2.26 | 1.29 | 5.5 | 6.6 | 2.7 | 3.3 |
| S1216 | 1.2 | 1.6 | 0.75 | 2.20 | 1.18 | 4.4 | 4.1 | 2.2 | 2.6 |
| S1515 | 1.5 | 1.5 | 1.0 | 2.45 | 1.45 | 8.4 | 8.4 | 2.8 | 3.6 |
| S1416 | 1.4 | 1.6 | 0.88 | 2.37 | 1.32 | 7.8 | 9.4 | 3.1 | 3.8 |
| S1317 | 1.3 | 1.7 | 0.76 | 2.39 | 1.20 | 6.4 | 6.4 | 2.4 | 3.1 |
| S1313 | 1.3 | 1.3 | 1.0 | 2.16 | 1.39 | 4.6 | 4.0 | 2.6 | 2.9 |
| S1214 | 1.2 | 1.4 | 0.86 | 2.08 | 1.24 | 4.1 | 3.8 | 2.5 | 2.8 |
| S1115 | 1.1 | 1.5 | 0.73 | 2.10 | 1.10 | 4.2 | 3.8 | 1.8 | 2.2 |
| C1216 | 1.2 | 1.6 | 0.75 | 2.34 | 1.19 | 4.5 | 3.4 | 1.9 | 2.4 |
| C1315 | 1.3 | 1.5 | 0.87 | 2.37 | 1.27 | 5.6 | 6.1 | 2.6 | 3.2 |
| P1315 | 1.3 | 1.5 | 0.87 | 2.13 | 1.28 | 5.9 | 4.0 | 2.4 | 2.8 |
| LS1414 | 1.4 | 1.4 | 1.0 | 3.67 | 1.81 | 11.1 | 2.5 | 1.0 | 1.4 |
| A151414 | 1.4 | 1.4 | 1.0 | 3.63 | 1.90 | 15.3 | 20.0 | 2.1 | 3.7 |
| A21414 | 1.4 | 1.4 | 1.0 | 3.45 | 1.90 | 16.0 | 19.2 | 2.2 | 3.8 |
| S1414co | 1.4 | 1.4 | 1.0 | 2.28 | 1.47 | 7.7 | 3.4 | 1.9 | 2.5 |
| S1414ct | 1.4 | 1.4 | 1.0 | 2.24 | 1.19 | 5.3 | 9.3 | 3.0 | 4.1 |
| S1216co | 1.2 | 1.6 | 0.75 | 2.23 | 1.13 | 4.6 | 0.6 | 0.8 | 1.0 |
| S1216ct | 1.2 | 1.6 | 0.75 | 2.14 | 1.11 | 3.6 | 5.7 | 2.7 | 3.3 |

The GW waveform $h_{ij}$ is extracted by making use of the quadrupole formula and is given by $h_{ij} = (2/D)d^2Q_{ij}/dt^2$, where $Q_{ij}$ is the Newtonian mass quadrupole and $D$ is the distance from the source (the indices $i$, $j$ denote the spatial directions). Compared to a more detailed extraction technique in the wave zone using the gauge-invariant Moncrief variables as done, e.g., in [4], this approximation is able to describe the GW signal only qualitatively. The wave phase and thus the frequency information can be well reproduced but the amplitudes are underestimated by about 30% in the inspiral regime and by about 40% in the post-merger regime [Fig. 12, panel (a) in [17]]. Based on the thus obtained waveform, the GW luminosity spectrum can be determined according to [18] by $dE_{GW}/df = \frac{\pi}{2}4\pi D^2 f^2 \langle |\tilde{h}_+|^2 + |\tilde{h}_\times|^2 \rangle$, where $\tilde{h}_+$ and $\tilde{h}_\times$ denote the Fourier transforms of the waveforms of "+" and "×" polarization, respectively. The angular brackets indicate

averaging over all possible source detection angles. The energy emitted in GWs is then given by $\Delta E_{GW} = \int df\, dE_{GW}/df$. Because of the underestimation of the GW amplitude, the GW luminosity spectra, which depend quadratically on the amplitude, are systematically too low by $\sim 70\%$.

Bearing this in mind, we consider in the following quantities that are not directly affected by this shortcoming and independent of the source orientation, namely (see Table I): (i) $f_{max}$ as the frequency of the GW signal when the amplitude becomes maximal at about the time of the final plunge. It is determined by fitting a function of the form $A(t)\cos[\omega(t)t + \phi]$ to the waveform, (ii) $f_{peak}$ as the frequency of the post-merger peak in the luminosity spectrum, (iii) the ratio $\Delta E_{in}/\Delta E_{pm}$ of $\Delta E_{in}$ as the energy emitted over a time interval of 3 ms before merging, and $\Delta E_{pm}$ as the energy radiated over a time interval of 5 ms after merging. The energies are determined as described above from the waveforms produced in the corresponding time intervals. The values thus obtained agree with time integrals of the quadrupole-formula-based expression $dE/dt = 1/5\langle \dddot{Q}_{ij}\dddot{Q}_{ij}\rangle$ to within $\sim 20\%$.

In cases where a HMNS forms, $f_{peak}$ turns out to depend sensitively on the EOS (Fig. 2, bottom) and to a lesser extent on the total mass of the binary system (Fig. 2, top). The NS spins and the mass ratio have very little influence
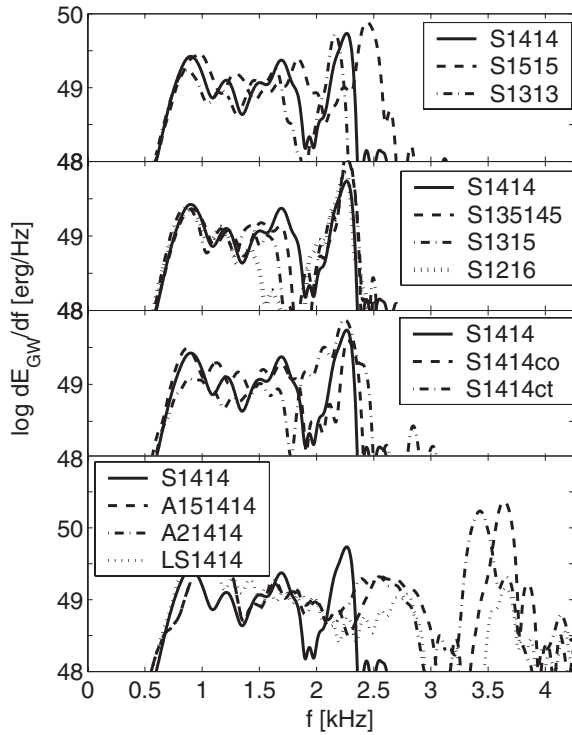


FIG. 2. GW luminosity spectra for different total masses, mass ratios, spin configurations, and EOSs (from top to bottom). Note that the spectrum below 1 kHz is not represented correctly because we started the simulations when the GW frequency was $\sim 1$ kHz.

(Fig. 2, middle panels). Indeed, all models using the Shen-EOS lead to values around 2.1–2.4 kHz for $f_{peak}$, where the variation among the Shen models of about 0.3 kHz is mostly due to the total system mass. On the other hand, the models using the APR-EOS and LS-EOS with their more compact NSs do not only yield larger values for $f_{max}$ [8,9] but also much larger ones (around 3.6 kHz) for $f_{peak}$. The latter quantity mainly depends on the behavior of the EOS in the density regime between $0.5\rho_0$ and $2\rho_0$ ($\rho_0 \approx 2.7 \times 10^{14}$ g cm$^{-3}$ being the nuclear saturation density), where the bulk of the remnant mass is located. While peak temperatures of several 10 MeV are present in the HMNS at such densities (see [7]), $T \neq 0$ contributions to the gas pressure affect the basic properties of the post-merger oscillations only moderately. A comparison of models C1315, C1216, and A151414 with S1315, S1216, and A21414, respectively, shows that $f_{peak}$ decreases by at most $\sim 0.2$ kHz when thermal pressure is included (Table I). This is caused by the less compact structure of the HMNS in these cases. Considering the radiated energies before and after merging, $\Delta E_{in}$ and $\Delta E_{pm}$, respectively, we find a characteristic variation of the GW signal with the NS spins. As shown in Fig. 3, the ratio of $\Delta E_{pm}$ to $\Delta E_{in}$ is highest for counterrotating cases and lowest for corotating NSs. This is so because corotation leads to a stronger inspiral signal due to a positive contribution from the NS spins, while damping the amplitude of the post-merger part due to a smaller nonaxisymmetry of the remnant [7]. Counterrotation has the opposite effect (cf. Fig. 1). The degeneracy of $f_{max}$ visible in Fig. 3 for cases with APR and LS-EOS can be lifted when the ratio $\Delta E_{pm}/\Delta E_{in}$ is taken into account.

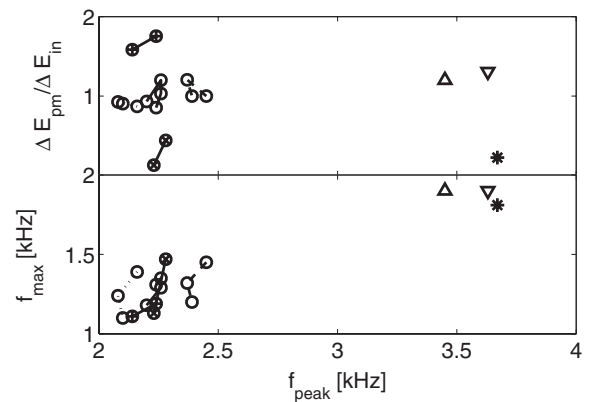A NS merger therefore produces a GW signal whose location in the space of the parameters $f_{max}$, $f_{peak}$, and



FIG. 3. Ratio $\Delta E_{pm}/\Delta E_{in}$ vs $f_{peak}$ (top) and $f_{max}$ vs $f_{peak}$ (bottom) for the models considered. Shen-EOS models are shown with a circle, APR-EOS models with triangles, and the LS-EOS model with a star. The two corotating models are indicated by $\times$, while the counterrotating models are marked with $+$. The horizontal spread of the model group with the Shen-EOS is mainly caused by different total system masses. Lines connect cases with the same total mass and spin setup.
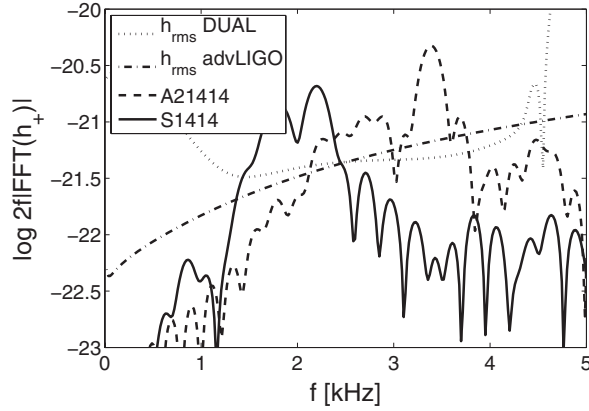
FIG. 4.   GW spectra $2f|\tilde{h}_+(f)|$ for two typical models with different EOSs, assuming a source distance of 20 Mpc. Also shown is the strain noise amplitude $h_{\rm rms}$ of advanced LIGO and of the resonant spheres detector DUAL.

$\Delta E_{\rm pm}/\Delta E_{\rm in}$ depends distinctively on the properties of the nuclear EOS. The latter determines the compactness of the merging stars and of the HMNS and thus the GW frequencies and energies emitted during the final plunge and post-merger oscillations. Characterizing a GW measurement in terms of the three parameters therefore provides direct information about the NS EOS, in particular, if the system mass is known from the inspiral chirp signal. This is a promising alternative to constraining the EOS by NS mass and very difficult radius determinations (e.g., [19] ). More work, however, is needed to understand the post-merger oscillations in terms of involved eigenmodes of the HMNS ([20] and references therein), and the GW parameters for a large variety of EOSs should be computed by accurate GR merger simulations.

To assess the detectability of the post-merger GW emission we follow Ref. [21] and consider the advanced LIGO interferometer and the omnidirectional DUAL detector, which consists of two nested resonant spheres [22]. The signal-to-noise ratio (SNR) for a given GW signal $h(t)$ can be written as $\text{SNR}^2 = \int_{-\infty}^{\infty} d\ln f |2f\tilde{h}(f)|^2/h_{\rm rms}(f)$, where $\tilde{h}(f)$ is the Fourier transform of $h(t)$ and $h_{\rm rms}(f)$ is the strain noise of the detector. In Fig. 4, we take $h(t) = h_+(t)$ and compare the spectrum $2f|\tilde{h}_+|$ for two representative models with the strain noise of the LIGO and DUAL instruments. For an interferometer, $h$ depends on the source orientation and direction relative to the interferometer arms and in the optimally aligned case is equal to $h_+$ or $h_\times$. For DUAL, $|\tilde{h}(f)|^2 = |\tilde{h}(f)_+|^2 + |\tilde{h}(f)_\times|^2$, because both polarizations can be measured simultaneously. In Table I the SNRs are listed for all of our models. Note that only the post-merger waveforms are considered and a distance of 20 Mpc is assumed. Since we have underestimated the wave amplitudes by ~40% (see above), our SNRs may be too low by up to a factor of 1.7. Moreover, the post-merger signals are likely to be emitted for longer times than the considered window of 5 ms. Fitting an exponential decay to the GW amplitudes, we find a decay

time of about 5 ms. From this, a further increase of the SNR by ~15% is estimated. Taking these corrections into account, we obtain for typical models like S1414 and APR21414 a SNR of ~5 in LIGO and ~6.5 in DUAL. Assuming that a minimal value of about 3 is needed for detection in case the preceding inspiral chirp has been measured, such GW signals may be identified up to ~35 Mpc (LIGO) and ~45 Mpc (DUAL). According to [2,23], these distances correspond to event rates of 0.04–0.5 (LIGO) and 0.08–1.1 (DUAL) per year.

[1]  K. Belczynski, V. Kalogera, and T. Bulik, Astrophys. J. **572**, 407 (2002).
[2]  V. Kalogera *et al.*, Astrophys. J. **601**, L179 (2004).
[3]  L. Blanchet, G. Faye, B. R. Iyer, and B. Joguet, Phys. Rev. D **65**, 061501 (2002).
[4]  M. Shibata and K. Taniguchi, Phys. Rev. D **73**, 064027 (2006).
[5]  M. Ruffert and H.-T. Janka, Astron. Astrophys. **380**, 544 (2001).
[6]  S. Rosswog and M. Liebendörfer, Mon. Not. R. Astron. Soc. **342**, 673 (2003).
[7]  R. Oechslin, H.-Th. Janka, and A. Marek, Astron. Astrophys. **467**, 395 (2007).
[8]  J. Faber, P. Grandclément, F. A. Rasio, and K. Taniguchi, Phys. Rev. Lett. **89**, 231102 (2002).
[9]  M. Shibata, Phys. Rev. Lett. **94**, 201101 (2005).
[10]  R. Oechslin, S. Rosswog, and F.-K. Thielemann, Phys. Rev. D **65**, 103005 (2002).
[11]  R. Oechslin, K. Uryū, G. Poghosyan, and F.-K. Thielemann, Mon. Not. R. Astron. Soc. **349**, 1469 (2004).
[12]  J. Isenberg and J. Nester, in *General Relativity and Gravitation*, edited by A. Held (Plenum, New York, 1980), Vol. 1, p. 23.
[13]  J. R. Wilson, G. J. Mathews, and P. Marronetti, Phys. Rev. D **54**, 1317 (1996).
[14]  H. Shen, H. Toki, K. Oyamatsu, and K. Sumiyoshi, Nucl. Phys. **A637**, 435 (1998).
[15]  J. M. Lattimer and F. D. Swesty, Nucl. Phys. **A535**, 331 (1991).
[16]  A. Akmal, V. R. Pandharipande, and D. G. Ravenhall, Phys. Rev. C **58**, 1804 (1998).
[17]  M. Shibata, K. Taniguchi, and K. Uryū, Phys. Rev. D **71**, 084021 (2005).
[18]  K. Thorne, *Three Hundred Years of Gravitation* (Cambridge University Press, Cambridge, England, 1987), Chap. 9.
[19]  J. M. Lattimer and M. Prakash, Phys. Rep. **442**, 109 (2007).
[20]  K. D. Kokkotas, T. A. Apostolatos, and N. Anderson, Mon. Not. R. Astron. Soc. **320**, 307 (2001).
[21]  E. E. Flanagan and S. A. Hughes, Phys. Rev. D **57**, 4535 (1998).
[22]  M. Cerdonio *et al.*, Phys. Rev. Lett. **87**, 031101 (2001).
[23]  C. Kim, V. Kalogera, and D. R. Lorimer, Astrophys. J. **584**, 985 (2003).